ACS APPLIED MATERIALS & INTERFACES

Research Article

www.acsami.org

High-Mobility Solution-Processed Tin Oxide Thin-Film Transistors with High-κ Alumina Dielectric Working in Enhancement Mode

Genmao Huang, Lian Duan,* Guifang Dong, Deqiang Zhang, and Yong Qiu

Key Lab of Organic Optoelectronics & Molecular Engineering of Ministry of Education, Department of Chemistry, Tsinghua University, Beijing 100084, P. R. China

Supporting Information

ABSTRACT: Solution-processed metal oxide thin-film transistors (TFTs) operating in enhancement mode are promising for the next-generation flat panel displays. In this work, we report high-mobility TFTs based on SnO_2 active layer derived from a soluble tin(II) 2-ethylhexanoate precursor. Densely packed polycrystalline SnO_2 thin films with moderate oxygen vacancies and only a few hydroxides are obtained via systemically optimizing precursor concentrations and processing conditions. The utilization of a solution-processed high-κ Al_2O_3 insulating layer could generate a coherent dielectric/semiconductor interface, hence further improving the device performance. TFT devices with an average field-effect mobility of 96.4 $cm^2\ V^{-1}\ s^{-1}$, a current on/off ratio of 2.2×10^6, a threshold voltage of 1.72 V, and a subthreshold swing of 0.26 V dec^{-1} have been achieved, and the driving capability is demonstrated by implementing a single SnO_2 TFT device to tune the brightness of an organic light-emitting diode. It is worth noting that these TFTs work in enhancement mode at low voltages less than 4 V, which sheds light on their potential application to the next-generation low-cost active matrix flat panel displays.

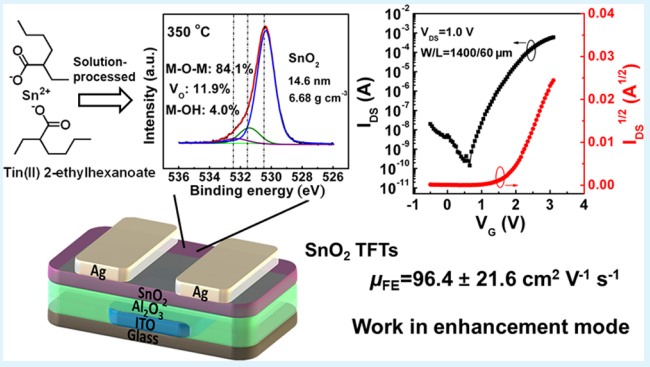

KEYWORDS: *thin-film transistor, solution-processed, tin oxide, enhancement mode, oxygen defects*

1. INTRODUCTION

Thin-film transistors (TFTs) are the key components for next-generation flat panel displays such as active-matrix organic light-emitting diodes (AMOLEDs).[1−3] In order to realize efficient current modulation, TFTs with high mobility and excellent stability are required for pixel-driving circuits. Thus, low-temperature polysilicon (LTPS) TFTs with mobility ∼200 $cm^2\ V^{-1}\ s^{-1}$ have been utilized to match with AMOLEDs.[4] However, the complex processing method and nonuniform device performance impede their large-scale application. So far, the emerging organic semiconductors could not yet compete with LTPS owing to their poor field-effect mobility (μ_{FE}) typically less than 1 $cm^2\ V^{-1}\ s^{-1}$.[5] On the other hand, metal oxide semiconductors have attracted tremendous attention due to their favorable field-effect mobility, high optical transparency, and robust chemical and thermal stability. TFTs based on metal oxide semiconductors with mobility exceeding 100 $cm^2\ V^{-1}\ s^{-1}$ have been achieved,[6−12] demonstrating their potential role as building blocks for AMOLEDs. Unfortunately, most of these high-mobility metal oxide TFTs were manufactured via processing methodologies based on vacuum apparatus with high capital investment, which are incompatible with low-cost, mass-producible future electronics. Therefore, a great deal of effort has been devoted to simple and inexpensive solution-processed metal oxide TFTs during the past decade.[13−18]

To date, solution-processed oxide TFTs incorporating indium exhibit impressive field-effect mobility, with noteworthy electron mobility of 44.2 $cm^2\ V^{-1}\ s^{-1}$ for indium zinc oxide (IZO),[19] 50 $cm^2\ V^{-1}\ s^{-1}$ for indium gallium zinc oxide (IGZO),[20] 113 $cm^2\ V^{-1}\ s^{-1}$ for zinc indium tin oxide(ZITO),[11] and 127 $cm^2\ V^{-1}\ s^{-1}$ for indium oxide (In_2O_3).[12] Nevertheless, indium is not a satisfactory candidate for mass production in view of the fact that indium is a rare element with low abundance in the earth crust. In this regard, considerable attempts have striven to search for indium-free oxide semiconductors with comparable or even better performance.[21−24] Tin is an element next to indium in the periodic table, and hence both Sn^{4+} and In^{3+} have the $[Kr]4d^{10}5s^0$ electronic configuration which is beneficial to electron transport because of large s-state spatial overlap.[25,26] Despite the extensive application of tin to ternary and quaternary oxides, studies on TFTs based on binary metal oxide SnO_2 are relatively scarce. TFTs based on SnO_2 active layer often exhibit a large off-current and even might not be modulated due to their high conductivity resulting from bulk or interfacial defects.[27] The progress on SnO_2 TFTs was frustrating during the past few years until recently Subramanian et al.[28] used a

Received: July 29, 2014
Accepted: November 6, 2014
Published: November 6, 2014

novel gel-like SnO_2 precursor containing $SnCl_2{\cdot}2H_2O$ and NH_4OH to deposit polycrystalline SnO_2 film. The combination of the SnO_2 active layer and high-κ ZrO_2 insulating layer brought about TFTs with a remarkable μ_{FE} over 40 $cm^2\ V^{-1}\ s^{-1}$.[29] However, such high mobility was achieved in devices working in depletion mode, which is incompatible with application in AMOLEDs. Even so, this work rekindled the interest in SnO_2 in oxide electronics.

High-quality thin films with low defect concentration are the prerequisite for high-performance oxide TFT devices operating in enhancement mode. To this end, selection of appropriate precursor materials and optimization of processing conditions should be carefully considered to grow oxide films with low defect fraction and smooth surface. Our previous study investigated the impact of Sn precursors on solution-processed zin tin oxide TFTs and found that tin(II) 2-ethylhexanoate could be a promising precursor material for metal oxide semiconductors.[30] Tin(II) 2-ethylhexanoate has been previously adopted to synthesize SnO_2 nanocrystals and fabricate tin oxide thin films for gas-sensing devices.[31−33] To our knowledge, there is no report on TFT device based on binary oxide semiconductor derived from this metalorganic precursor.

In this work, we prepared TFTs based on SnO_2 active layer via spin-coating from precursor solution by dissolving tin(II) 2-ethylhexanoate in xylene. Impact of precursor concentration and processing temperature on film formation process was initially investigated, and the optimal SnO_2 thin film with a high density of 6.68 g cm^{-3} and low oxygen defect fraction was obtained. With solution-processed high-κ Al_2O_3 serving as insulating layer, a coherent dielectric/semiconductor interface along with smooth surface could be generated, which results from the combined effect of smooth Al_2O_3 substrate and Al-doping into semiconductor layer during thermal annealing. TFT devices with an average mobility of 96.4 $cm^2\ V^{-1}\ s^{-1}$, a current on/off ratio of 2.2×10^6, a threshold voltage of 1.72 V, and a subthreshold swing of 0.26 V dec^{-1} were achieved. Fortunately, these TFTs operate in enhancement mode at low voltages less than 4 V. We also employed a single SnO_2 TFT device to tune the brightness of an OLED and confirmed its effective current switching and modulation capability in pixel driving. These high-quality devices with the current state-of-art mobility in solution-processed SnO_2 TFTs enable the potential for the next-generation low-cost active-matrix flat panel displays.

2. EXPERIMENTAL SECTION

Precursor Solution Preparation. SnO_2 precursor solutions were prepared by dissolving tin(II) 2-ethylhexanoate (Alfa Aesar, 99.5%) in xylene with concentrations of 0.15 and 0.3 M, respectively. Al_2O_3 precursor solution was prepared by dissolving aluminum nitrate nonahydrate (Strem Chemicals, 99%) in 2-methoxyethanol with a concentration of 0.5 M. All the chemicals were used as received without further purification.

Film Deposition. Prior to spin-coating, all the precursor solutions were stirred for 12 h at room temperature and then filtered through 0.22 μm nylon syringe filters. To deposit SnO_2 films, the prepared SnO_2 precursor solutions were spin-coated at 3000 rpm for 30 s, dried at 180 °C on a hot plate for 5 min to remove solvent, and then annealed at different temperatures for 30 min. To form the Al_2O_3 insulating layer, the alumina precursor was spin-coated at 3000 rpm for 30 s and subsequently baked at 220 °C for 5 min, and then another spin-coating and baking cycle was repeated, followed by the postannealing step at 450 °C for 30 min. The spin-coating processes were performed in a nitrogen glovebox, and the annealing processes were carried out in ambient.

Device Fabrication. Bottom-gate top-contact transistors were fabricated on glass substrates with patterned indium tin oxide (ITO) used as gate electrode. The substrates were cleaned with detergent and deionized water, successively. Alumina gate dielectric and SnO_2 semiconductor layer were deposited in sequence as above. Ag or Au source and drain electrodes with a thickness of 80 nm were deposited via thermal evaporation in vacuum at 10^{-6} Torr through a shadow mask. The channel length and width are 60 and 1400 μm, respectively.

Characterization. The thermal behavior of SnO_2 precursor solution was monitored under an ambient atmosphere using a thermal gravimetric and a differential scanning calorimeter (TGA-DSC, NETZSCH, STA449F3) with a heating rate fixed at 10 °C/min. Variation in the chemical compositions of SnO_2 films were observed using a Fourier transform infrared spectrometer (FT-IR, Vertex 70, Bruker Optic). The crystalline property of the SnO_2 films was determined by grazing incidence angle X-ray diffraction (GIXRD, BSRF 1W1A) based on synchrotron radiation light source, using a fixed glancing incidence angle of 0.3°. The composition of films was examined by X-ray photoelectron spectroscopy (XPS, Thermo Scientific, ESCALAB 250Xi) and Auger electron spectroscopy (AES, ULVAC-PHI, PHI-700). The optical property of films was measured with a UV−visible spectrometer (Agilent 8453). The density of films was analyzed by X-ray reflectivity (XRR, Bruker D8 Discover) at a wavelength of 0.154 nm. The thickness of thin films was characterized by field-emission scanning electron microscope (SEM, HITACHI, S-4800) and XRR. Surface morphology of films was examined by atomic force microscope (AFM, Seiko, SPA400) and SEM. The cross-sectional multilayer structures were observed by high-resolution transmission electron microscope (HRTEM, FEI, G20). The capacitance per area (C_i) was obtained with a precision impedance analyzer (Agilent, 4294A) by measuring capacitance-frequency properties of the device with ITO/Al_2O_3/Ag structure. The electrical characteristics of TFTs were performed with a semiconductor characterization system (Keithley, 4200SCS) under ambient condition.

3. RESULTS AND DISCUSSION

To understand the conversion process from liquid metalorganic precursor to solid SnO_2 film, systematic investigations including TGA-DSC, FT-IR, XRR, GIXRD, and XPS analysis were carried out, and these relevant results are summarized in Table 1. TGA-DSC measurement was initially performed as shown in Figure 1a. The sample for thermal analysis was prepared by mild drying of SnO_2 precursor solution comprised of tin(II) 2-ethylhexanoate and xylene. The mass loss below 200 °C represented the evaporation of residual solvent and partial decomposition of tin(II) 2-ethylhexanoate. Drastic mass loss was monitored between 250 and 320 °C, indicating the gradual conversion from decomposed organometallic compound to metal oxide. Meanwhile, crystallization process of SnO_2 film could be identified in the DSC curve characterized by a broad exothermic peak appearimg around 300 °C and centered at 356 °C.

Table 1. Density, Thickness, Crystalline Property, and Composition of SnO_2 Thin Films Annealed at Different Temperatures

temp (°C)	density (g cm^{-3})	thickness (nm)	crystalline property	M−O−M (%)	V_o (%)	M−OH (%)
180	3.98	18.9	amorphous	46.7	39.9	13.4
250	4.38	16.7	amorphous	57.2	27.4	15.4
300	5.01	14.9	amorphous	67.6	24.9	7.5
350	6.68	14.6	polycrystalline	84.1	11.9	4.0
450	6.59	12.2	polycrystalline	81.0	12.1	6.9

dx.doi.org/10.1021/am5050295 | ACS Appl. Mater. Interfaces 2014, 6, 20786−20794

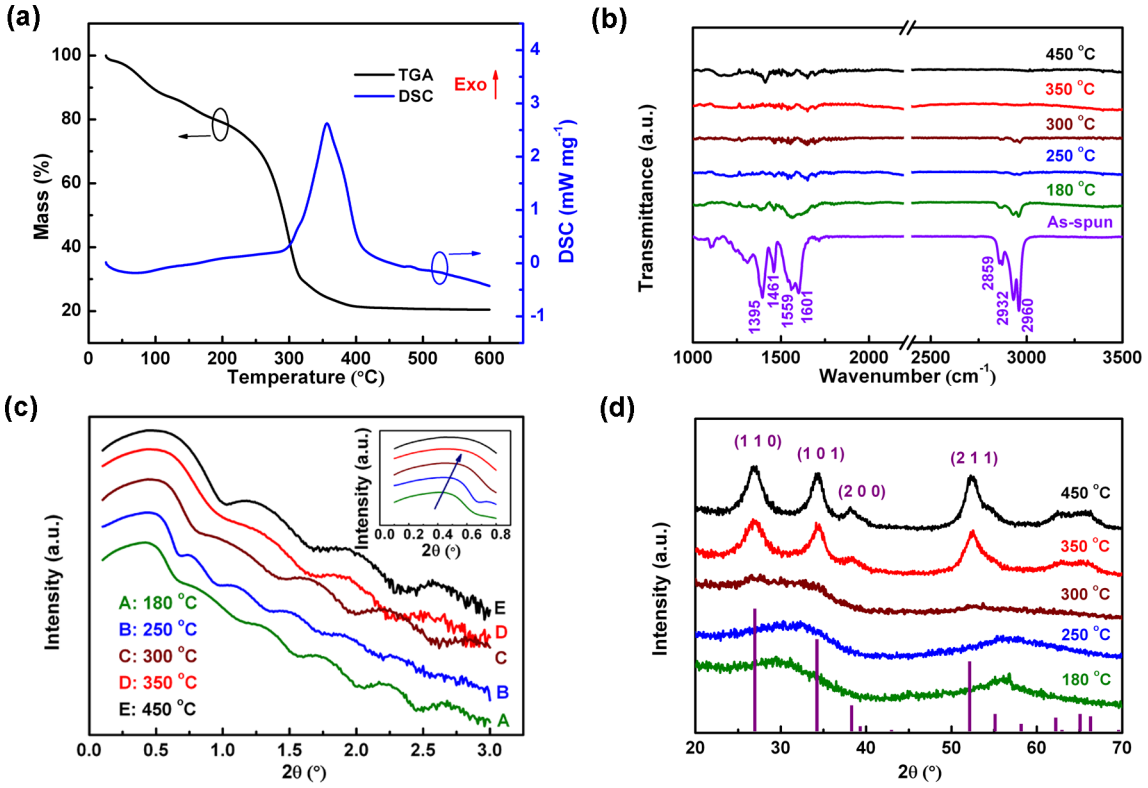

Figure 1. (a) TGA-DSC curves of the precursor solution sample. (b) FT-IR, (c) XRR, (d) GIXRD analysis of SnO_2 films fabricated with various annealing temperatures. Inset in (c): enlarged graph of data relevant to critical angles (arrow), showing variation of film density.

Figure 1b shows the FT-IR spectra of films treated with different heating temperatures. The as-spun film exhibited strong absorption peaks due to organic ligands of tin(II) 2-ethylhexanoate and residual solvent. The intensive peaks at 1395 and 1601 cm^{-1} were mainly assigned to the symmetric and asymmetric stretchings of carboxylate, respectively, and the absorptions in the 2859−2960 cm^{-1} region arose from the stretching modes of C−H vibrations.[33−35] These peaks were also manifest in the sample heated at 180 °C, implying large amount of organic residuals existing owing to the incomplete conversion process. With annealing temperature reaching above 350 °C, most organic impurities could be removed whereas few residuals inevitably remained in SnO_2 film. As for carrier transport in metal oxide, organic impurities generally act as acceptor traps,[1] resulting in enhanced carrier scattering and hence reduced mobility. Besides, with regard to the TFT device, impurities are believed to cause trapping/detrapping of electrons during the gate voltage sweep and thus induce hysteresis.[36] Therefore, it is a key issue to determine an appropriate temperature for fabricating high-quality SnO_2 thin films.

The density and thickness of thin films annealed at temperatures ranging from 180 to 450 °C were determined by XRR analysis, depicted in Figure 1c. The critical angles related to film density for total external reflection of the 350 and 450 °C-annealed SnO_2 films were almost the same, and significantly larger than the other three samples. According to Buydens' method,[37] the deduced densities of films annealed at 350 and 450 °C were 6.68 and 6.59 g cm^{-3}, respectively. These densities are comparable to the previously reported values of dense SnO_2 films deposited via vacuum-based apparatus, and close to the theoretical density of bulk SnO_2 of 6.95 g cm^{-3}.[38−40] As expected, the 180 °C-treated film had the minimal density of 3.98 g cm^{-3}, while the densities of films annealed at 250 and 300 °C increased to 4.38 and 5.01 g cm^{-3}, respectively. The Kiessig fringes were discernible in XRR patterns, and thus the thickness of each film could be calculated from two individual interference maxima.[41] As the annealing temperature rose from 180 to 450 °C, the thickness of SnO_2 thin film declined from 18.9 to 12.2 nm, which complied with the densification process of these SnO_2 thin films.

Figure 1d shows the GIXRD patterns of SnO_2 thin films treated with different annealing temperatures. SnO_2 films obtained at 350 and 450 °C were polycrystalline, while the other three samples were amorphous. The distinct peaks at 2θ near 26.6°, 33.9°, 37.9°, and 51.8° represented (110), (101), (200), (211) crystal planes of cassiterite SnO_2 (JCPDS no. 41-1445), respectively.[27,28,31] The temperature-dependent crystalline property is in agreement with the above-mentioned TGA-DSC analysis, and it could be confirmed that the crystalline phase conversion of SnO_2 film occurred between 300 and 350 °C. Thereby, annealing at 350 °C for 30 min is sufficient to accomplish the crystallization of SnO_2 microstructure.

Oxygen defects, including oxygen vacancies and hydroxides, in semiconducting layer play an important role in charge carrier transport by affecting field-effect mobility and threshold voltage of TFTs. XPS measurement was performed to understand the local bonding structural differences among these films, and the results are depicted in Figure 2a and Figure S1 (see Supporting Information). After all binding energies were corrected with reference to the C_{1s} line at 284.8 eV for sample charging effect, the O_{1s} peaks were deconvoluted into three principal subpeaks using Gaussian−Lorentzian profile. The binding energy peak at 530.4 eV was attributed to M−O−M lattice species without oxygen defects, the feature at 531.7 eV was assigned to the oxygen vacancies (V_o) in the oxide lattices, and the peak

dx.doi.org/10.1021/am5050295 | ACS Appl. Mater. Interfaces 2014, 6, 20786−20794

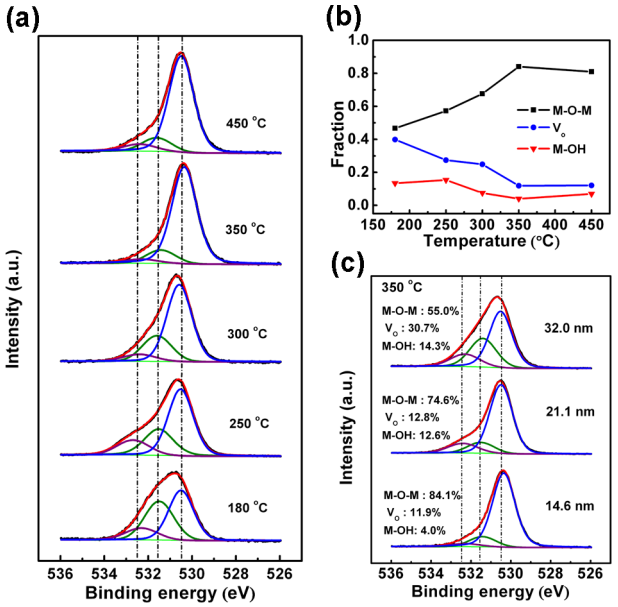

Figure 2. (a) O_{1s} XPS peak of SnO_2 films annealed at temperatures ranging from 180 to 450 °C. (b) Semiquantitative analysis of the fraction of M−O−M, V_o, and M−OH as a function of the annealing temperature. (c) O_{1s} XPS peak of SnO_2 films with different thickness annealed at 350 °C. All fractions were calculated based on the area integration of each subpeak.

centered at 532.3 eV could be associated with the oxide in hydroxide (M−OH), which was caused by the absorbed H_2O, O_2, or OH species on the surface.[42] The fractions of each composition for different SnO_2 films treated with annealing temperatures ranging from 180 to 450 °C are summarized in Figure 2b. It could be found that the fraction of M−O−M increased from 46.7% to 84.1% as annealing temperature increased from 180 to 350 °C, while the proportions of V_o and M−OH declined from 39.9% to 11.9% and 13.4% to 4%, respectively. Compared with the 350 °C-treated sample, the film annealed at 450 °C contained slightly higher amount of V_o and M−OH. This deviation might probably originate from loss of metal atoms during high-temperature annealing process.[30,43] Previous reports suggested that M−O−M backbones in metal oxide serve as electron conductance pathways, whereas M−OH acts as traps and hinders electron transport.[15,44] Adequate amount of V_o is known to offer free electrons and is beneficial to mobility boost.[3,6] However, excess free electrons may give rise to a highly conductive film and make it difficult to achieve normally off-operation with regard to TFT device application.[27,45] Therefore, the fraction of oxygen defects should be restricted to an appropriate level so as to achieve enhancement-mode TFT device.

The effect of film thickness on density and oxygen defects of SnO_2 films annealed at 350 °C was further studied. Thicker SnO_2 films with thickness of 32.0 and 21.1 nm were fabricated by single spin-coating process either from precursor solution with higher concentration or based on different processing condition. These thicker films exhibited lower density less than 5 g cm^{-3} (see Supporting Information Figure S2) and had significantly higher oxygen defect fraction compared with the 14.6 nm SnO_2 film, as shown in Figure 2c. As the film thickened from 14.6 to 32.0 nm, the fraction of M−O−M diminished from 84.1% to 55.0%, while the proportion of M−OH rose from 4.0% to 14.3%. With respect to these thicker films, the increased number of pores and pinholes would lead to higher bulk defect concentration, and hence affect charge transport properties.[46]

The optical transmittance and bandgap of 350 °C-treated SnO_2 films deposited on quartz substrate were investigated (see Supporting Information Figure S3). From the optical transmittance, either the 14.6 nm or the 32.0 nm-thick SnO_2 thin film exhibited high transmittance over 95% in the visible region. The estimated optical bandgap (E_g) of SnO_2 films extracted from the Tauc's plot was ∼3.6 eV, consistent with previous reports.[2,42] The thickness of 350 °C-treated SnO_2 film derived from 0.15 M precursor solution was further verified by cross-sectional SEM image of $Si/SiO_2/SnO_2$ structure to be about 15 nm (see Supporting Information Figure S4), close to the value calculated from XRR analysis. On account of aforementioned results, such dense polycrystalline SnO_2 thin film with low defect concentration was chosen for further TFT device fabrication.

High-κ dielectric materials which induce high carrier concentration at low voltage have been often incorporated to enable high-performance TFTs. Thanks to the advantages of high relative permittivity, wide energy gap, and smooth amorphous surface, aluminum oxide (Al_2O_3) has been widely used as insulating layer in TFTs.[12,19,24] In this work, solution-processed Al_2O_3, prepared according to the procedure reported by Xia et al.,[47] was utilized as the gate dielectric. The amorphous structure and smooth surface were verified by GIXRD and AFM, respectively (see Supporting Information Figure S5), and the C_i values were measured to be 182 and 87 nF cm^{-2} at low frequency of 40 Hz and at high frequency of 10 kHz, respectively (see Supporting Information Figure S6). Since mobile ions existing in solution-processed metal oxide gate dielectrics would enable slow polarization over long time scales,[22] result in the formation of electrical double layer, and lead to the variation of capacitance with applied frequency, known as dispersive behavior,[29] the value of capacitance should be carefully chosen for mobility calculation. Because TFT characterization is performed in direct voltage, the measured or extrapolated capacitance value at a relatively low frequency was often adopted for device mobility calculation.[19,20] In this work, the C_i value of 225 nF cm^{-2} extrapolated to 1 Hz, acquired from average capacitance-frequency curve (see Supporting Information Figure S6d), was used to calculate field-effect mobility according to previous reports.[20,23]

The interface between gate dielectric and semiconductor is crucial to TFT device performance. In particular, switching speed is associated with the density of interface states. Supporting Information Figure S7 shows the cross-sectional electron microscope images of Al_2O_3/SnO_2 structure. The thickness of Al_2O_3 and SnO_2 were about 100 and 15 nm, respectively. As depicted in Figure 3a, the cross-sectional TEM image clearly demonstrated a uniform and smooth interface between Al_2O_3 and SnO_2 layers, which is beneficial to electron transport. The SnO_2 lattice fringes could also be seen in the HRTEM image. The energy dispersive X-ray spectroscopy (EDX) analyses, including profile and mapping modes, were carried out to qualitatively describe element distribution in such sample (see Supporting Information Figures S8, S9). Further, the depth profile of $ITO/Al_2O_3/SnO_2$ stack was analyzed via Auger electron spectroscopy with Ar sputtering etching. Figure 3b shows the element content variation while etching from the top of the sample, with atomic concentration of Sn, O, Al, and In being examined. With respect to the Al_2O_3/SnO_2 interface,

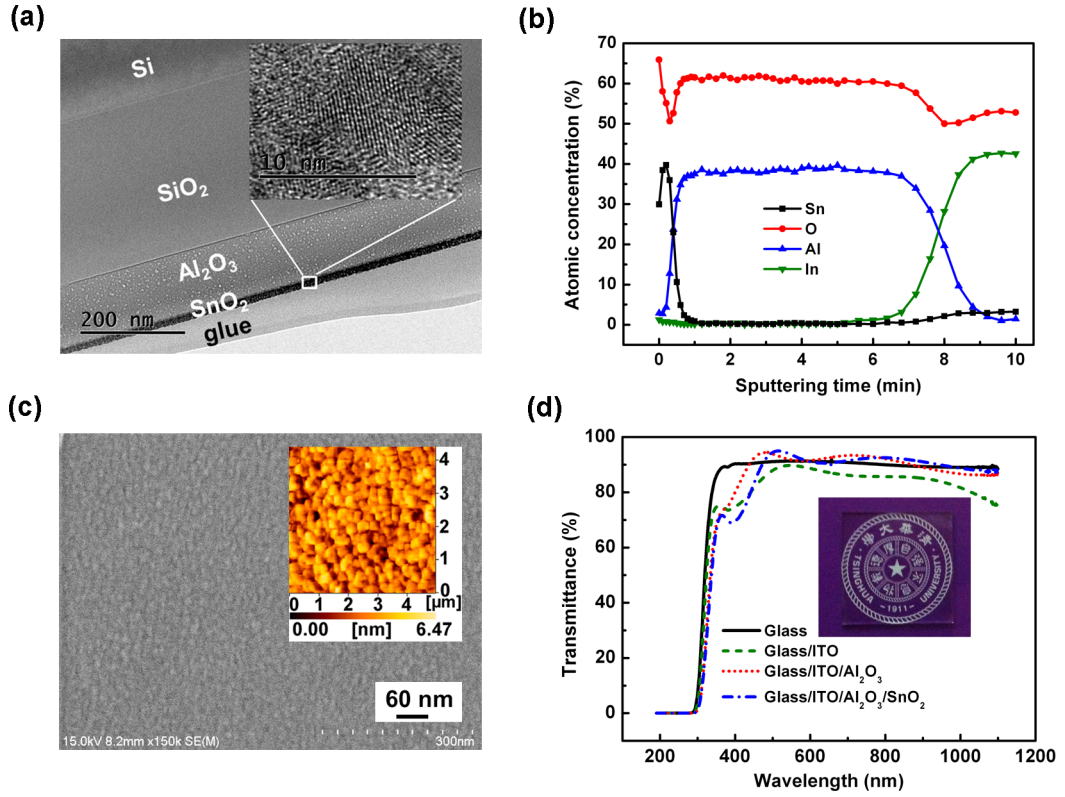

Figure 3. (a) Cross-sectional TEM image of $Si/SiO_2/Al_2O_3/SnO_2$ structure. Inset: HRTEM image of SnO_2, scale bar: 10 nm. (b) AES depth profile with Sn, O, Al, and In being investigated in $ITO/Al_2O_3/SnO_2$ stack. (c) SEM image of the surface of the SnO_2 film deposited on ITO/Al_2O_3 substrate. Inset: AFM image of the SnO_2 film deposited on ITO/Al_2O_3 substrate. (d) Optical transmittance of multiple stacks. Inset: photograph of the $ITO/Al_2O_3/SnO_2$ stack, showing excellent transparency.

we can clearly observe the diffusion of Al into SnO_2 film with a long diffusion depth. In contrast to an abrupt heterogeneous interface, a coherent interface enables defect relaxation[22] such as eliminating interfacial lattice mismatch. Moreover, previous reports suggested that the Al-doping effect could suppress carrier concentration.[48,49] Accordingly, in this work, the diffusion of Al into active layer would reduce the amount of weakly bonded oxygen atoms, hence suppressing intrinsic excess free carriers.

Figure 3c shows the surface morphology of the SnO_2 layer on ITO/Al_2O_3 substrate. SEM image revealed that the SnO_2 microstructure was composed of closely packed particles and free of obvious pores or pinholes, and the extracted root-mean-square (rms) roughness value for SnO_2 was 0.97 nm according to AFM analysis. This smooth polycrystalline surface was attributed to the coaction of ultrasmooth underlying Al_2O_3 substrate with rms of 0.29 nm (see Supporting Information Figure S5) and unintentional Al-doping effect during thermal annealing. This smooth and compact SnO_2 film provides favorable surface for source and drain electrodes contact, which could avoid device performance degradation owing to poor surface of polycrystalline active layer.

The optical transmittance of multiple stacks was measured as illustrated in Figure 3d. For stacks with either ITO/Al_2O_3 or $ITO/Al_2O_3/SnO_2$ structure, the average transmittance in the visible range was around 90%. Interestingly, compared with the bare ITO substrate, a notable improvement in transparency of either structure was observed. The enhancement of light extraction presumably originates from a better refractive index matching at the interfaces of ITO (n = 1.8)/Al_2O_3 (1.55)/air (n = 1.0) than that at the ITO/air interface (the refractive index of Al_2O_3 was measured by ellipsometer at a wavelength of 632 nm), which reduced the total internal reflection at the interface.[50] Moreover, Pinto et al.[51] suggested that rough substrate leads to a decrease in transmittance due to stronger light scattering. Therefore, the improved surface with reduced roughness after either Al_2O_3 or Al_2O_3/SnO_2 deposition was also responsible for improved light extraction. The high optical transmittance of glass/$ITO/Al_2O_3/SnO_2$ structure in this work offers potential application to transparent electronics.

Bottom-gate top-contact thin-film transistors were fabricated, and the structure is illustrated in Figure 4a. Thermally evaporated Ag, patterned through a shadow mask, was used as source and drain (S/D) electrodes to afford a channel dimension of L = 60 and W = 1400 μm (see Supporting Information Figure S10). This W/L ratio was carefully selected to limit the overestimation of field-effect mobility. It has been reported that a small W/L ratio of 5 may induce mobility overestimation up to ~200%,[52] whereas the overestimation dropped to 10% with W/L ratio increased to 10.[11] Herein, the large W/L ratio over 20 in this work could efficiently limit mobility overestimation. Figure 4b shows the representative output characteristic curve of a TFT device with clear pinch-off and current saturation behavior at low-voltage region.

Figure 4c shows the representative transfer characteristic curve of one of our TFTs at V_{DS} = 1 V as a function of V_G sweeping from −0.5 to 3.0 V. The transfer plot indicated the n-type transistor behavior of the semiconducting SnO_2. We also fabricated TFTs based on commonly used Au S/D electrodes to investigate the influence of electrode work function on TFT

dx.doi.org/10.1021/am5050295 | ACS Appl. Mater. Interfaces 2014, 6, 20786−20794

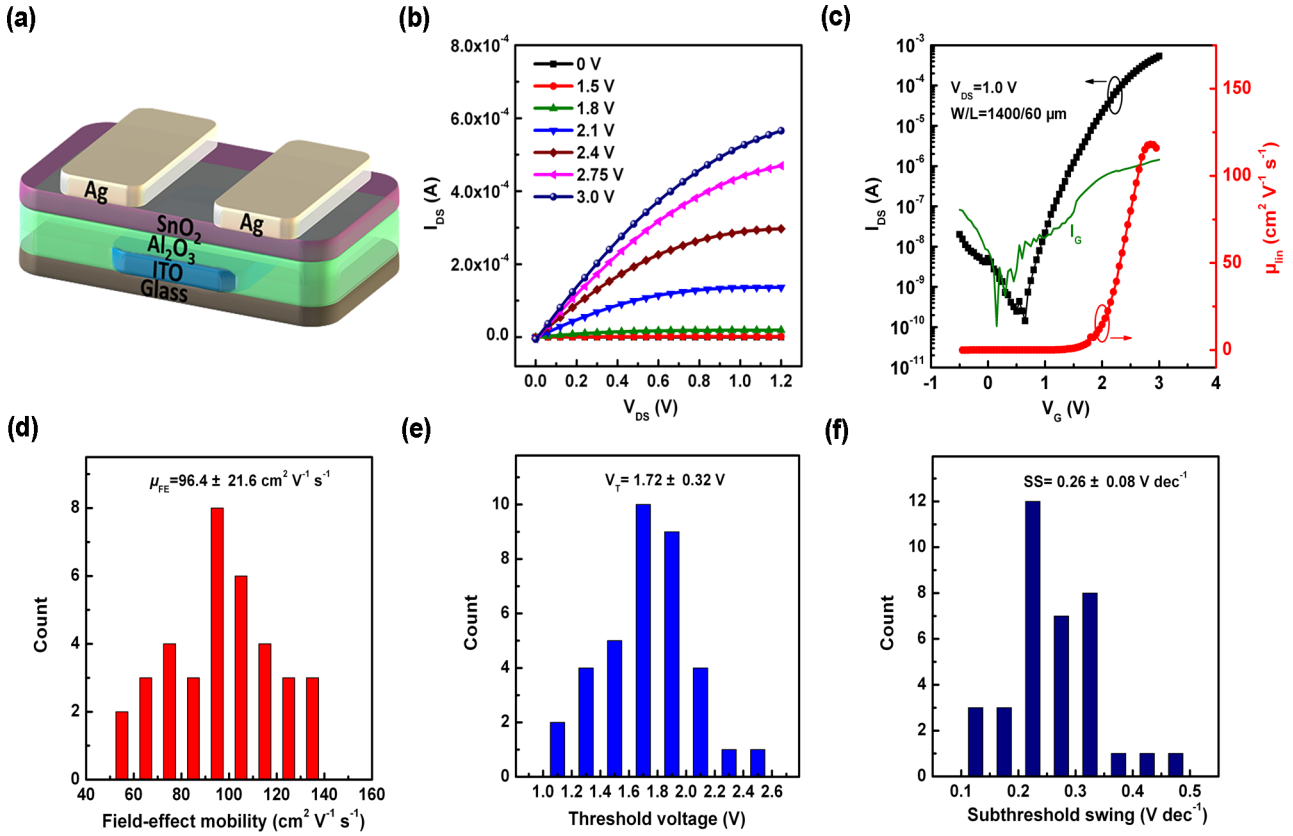

Figure 4. (a) Schematic illustration of TFT devices used in this study (not drawn to scale). (b) Output plot of the representative TFT. (c) Transfer plot of the representative TFT. (d–f) Histograms of field-effect mobility, threshold voltage, and subthreshold swing based on 36 TFT devices.

performance (see Supporting Information Figure 11). Since there is no significant difference of transconductance between the two types of devices, TFTs with Ag S/D electrodes were performed to assess uniformity and reproducibility in terms of cost-effectiveness. Thirty-six TFT devices were measured in ambient, and the field-effect mobility (μ_{lin} for linear region and μ_{sat} for saturation region), current on/off ratio ($I_{on/off}$), threshold voltage (V_{th}), and subthreshold swing (SS) of these TFTs could be acquired from transfer plots and according to the reported equations[2,14]

$$\mu_{lin} = \frac{L}{WC_iV_{DS}}\left(\frac{\partial I_{DS}}{\partial V_G}\right) \quad (1)$$

$$\mu_{sat} = \frac{2L}{WC_i}\left(\frac{\partial \sqrt{I_{DS}}}{\partial V_G}\right)^2 \quad (2)$$

$$SS = \frac{dV_G}{d(\lg I_{DS})} \quad (3)$$

where L and W are the channel length and width, respectively, C_i is the capacitance per unit area of the dielectric layer, V_{DS} is the drain-to-source voltage, I_{DS} is the drain-to-source current, and V_G is the gate-to-source voltage. In order to limit overestimation of the extracted field-effect mobility, we adopted the extrapolated C_i value of 225 nF cm^{-2} for mobility calculation.

These 36 TFT devices exhibited similar performance for μ_{FE} (96.4 ± 21.6 cm^2 V^{-1} s^{-1}), $I_{on/off}$ (2.02 (±2.63) × 10^6), V_T (1.72 ± 0.32 V), and SS (0.26 ± 0.08 V dec^{-1}). The histograms of these parameters are shown in Figure 4d–f. The standard deviations of these merits are generally inferior to amorphous TFTs because of the grain boundary effect, but these results still proved that acceptable overall device uniformity and yield could be obtained based on polycrystalline SnO_2 TFTs in this work.

The electrical performance of TFT device depends on the quality of thin films integrated in the device. In this work, dense polycrystalline SnO_2 thin film with reduced M–OH fraction less than 5% was obtained via wisely choosing precursor material and systematically optimizing precursor concentrations and processing temperatures. The fabrication process from precursor solution to TFT device inhibited the formation oxygen defects such as hydroxides acting as traps, and hence facilitated electron transport in the active layer. Further, the utilization of smooth high-κ Al_2O_3 insulating layer not only offered a high-quality Al_2O_3/SnO_2 interface leading to a small SS value but also contributed to low-voltage operation behavior originating from the high capacitance of the dielectric layer. Previous studies revealed mobility boost of 5–20× by using high-κ gate dielectrics instead of thermally grown SiO_2.[9,11,28] According to the reports, it seems that the employment of high-κ Al_2O_3 insulating layer also contributes to the high mobility of these SnO_2 TFTs. However, the utilization of Al_2O_3 dielectric should not be ascribed to the dominant factor for the high mobility in our work. TFTs based on the same configuration with SnO_2 film obtained from anhydrous tin chloride ($SnCl_2$) precursor material were fabricated, exhibiting much inferior μ_{FE} less than 10 cm^2 V^{-1} s^{-1} (see Supporting Information Figure S12). Compared with the tin(II) 2-ethylhexanoate precursor, chloride-derived SnO_2 film was rather rough and contained

dx.doi.org/10.1021/am5050295 | ACS Appl. Mater. Interfaces 2014, 6, 20786–20794

more oxygen defects (see Supporting Information Figure S13). Such deterioration is considered to be involved with different TGA behavior and oxide film formation mechanism.[30] Therefore, the adoption of metalorganic precursor material and the adapted processing condition is assumed to be the primary reason for mobility boost in this work. The high mobility of the optimized SnO_2 TFTs should be attributed to the combined effect of high-quality active layer, high-capacitance dielectric layer, and a coherent dielectric/semiconductor interface.

TFT devices with active layer derived from 450 °C-treated tin(II) 2-ethylhexanoate were also fabricated, and the electrical performance is shown in Supporting Information Figure S14. Compared with TFTs based on 350 °C-treated active layer, there was about 10%−20% reduction in mobility of the 450 °C devices, which is assumed to be resulted from a higher content of M−OH, known as charge trap sites.[15] The mobility of 450 °C device still remains at a high level among solution-processed metal oxide TFTs, indicating the optimal temperature can have a relatively large window.

We noticed there were reliability issues such as gate leakage current (I_G) and hysteresis behavior (see Supporting Information Figure S15) in our TFT devices. In the low gate voltage region where $V_G < 1$ V, the I_G was even larger than I_{DS} because the conductive channel was not formed.[11] However, the I_G would not lead to overestimation of mobility since it was far less than 1% of I_{DS} in the saturation region.[53] As for the hysteresis, Jang et al.[24] concluded that trapping at the localized states at the sol−gel-Al_2O_3/semiconductor interface other than bulk phase caused instability of the TFT. Our studies focusing on overcoming these drawbacks are underway.

As can be extrapolated from the transfer plot in Figure 4c, the values of turn-on voltage (V_{on}) and V_T were 0.6 and 1.7 V, respectively, indicating the enhancement-mode operation of the TFT device. Besides, negligible $I_{DS} \sim 10^{-9}$ A flowed through the channel at $V_G = 0$, which was satisfactory with the requirement to turn off an OLED pixel under no bias voltage. Compared with previous reports on enhancement-mode SnO_2 TFTs suffering from low field-effect mobility,[27,54] our devices overcome this issue. In contrast to most previously reported SnO_2 TFTs operating in depletion mode,[10,28,55] the 14.6 nm SnO_2 thin film with moderate V_o content and extremely low M−OH fraction presumably limited free carrier concentration and ensured a low off-current, thus leading to the enhancement-mode operation of our TFT devices. Our attempt to use a 32.0 nm defect-rich SnO_2 thin film aiming at enhancement-mode operation failed featured by a large off-current, probably due to increased amount of defects in a thicker active layer (see Supporting Information Figure S16).[27]

We eventually implemented a single SnO_2 TFT device to tune the brightness of a bottom-emitting OLED pixel in a series circuit, as depicted in Supporting Information Figure S17. With source electrode grounded and drain electrode of the SnO_2 TFT connected to the cathode of the OLED, a varying V_G and a constant V_{DS} were applied to the TFT device. As the V_G swept forward from 0 V to maximum 4 V and backward to 0 V, the OLED pixel underwent gradually enhanced electroluminescence and a reverse process to off-state. This prototype demonstrated efficient current switching and modulation of our SnO_2 TFT. Further improvement involved with active-matrix circuit is under progress.

4. CONCLUSION

In conclusion, we have prepared high-mobility enhancement-mode TFTs based on solution-processed SnO_2 thin film using tin(II) 2-ethylhexanoate as precursor material. Densely packed polycrystalline SnO_2 thin films with moderate oxygen vacancies and only a very few hydroxides could be obtained by optimizing precursor concentration and processing temperature. The utilization of solution-processed high-κ Al_2O_3 as the insulating layer to match with SnO_2 active layer could contribute to a coherent dielectric/semiconductor interface, attributed to the coaction of smooth Al_2O_3 substrate and Al-doping into active layer during thermal annealing. TFT devices with an average μ_{FE} of 96.4 $cm^2 V^{-1} s^{-1}$, I_{on}/I_{off} of 2.2×10^6, V_T of 1.72 V, and SS of 0.26 V dec^{-1} were achieved, and the pixel driving prototype was demonstrated by implementing a single SnO_2 TFT device to tune the brightness of an organic light-emitting diode. It is noteworthy that these TFTs could operate in enhancement mode at low voltages less than 4 V, which sheds light on their potential application to the next-generation low-cost active matrix flat panel displays.

■ ASSOCIATED CONTENT

Ⓢ Supporting Information

XPS survey scan and Sn 3d spectra, XRR analysis, optical transmittance, cross-sectional SEM image of single SnO_2 layer; characterization of Al_2O_3 gate dielectric; electron microscope images and EDX analyses of cross-sectional Al_2O_3/SnO_2 structures; characterization of SnO_2 thin film derived from $SnCl_2$ precursor; output and transfer characteristics of devices based on Au S/D electrodes, 450 °C-treated tin(II) 2-ethylhexanoate precursor, $SnCl_2$ precursor, and defect-rich SnO_2 active layers; driving prototype of a single TFT implemented to tune the brightness of an OLED. This material is available free of charge via the Internet at http://pubs.acs.org/.

■ AUTHOR INFORMATION

Corresponding Author

*Tel.: +86 10 62779988. Fax: +86 10 62795137. E-mail address: duanl@mail.tsinghua.edu.cn.

Notes

The authors declare no competing financial interest.

■ ACKNOWLEDGMENTS

We thank the National Natural Science Foundation of China (Grant Nos. 51173096, 21161160447, and 61177023) for financial support. The GIXRD data of this work were obtained at 1W1A beamline, Beijing Synchrotron Radiation Facility (BSRF). The authors gratefully acknowledge the assistance of scientists of Diffuse X-ray Scattering Station during the experiments.

■ REFERENCES

(1) Barquinha, P.; Martins, R.; Pereira, L.; Fortunato, E. *Transparent Oxide Electronics: From Materials to Devices*; Wiley: Chichester, U.K., 2012.

(2) Fortunato, E.; Barquinha, P.; Martins, R. Oxide Semiconductor Thin-Film Transistors: A Review of Recent Advances. *Adv. Mater.* **2012**, *24*, 2945−2986.

(3) Park, J. S.; Maeng, W. J.; Kim, H. S.; Park, J. S. Review of Recent Developments in Amorphous Oxide Semiconductor Thin-Film Transistor Devices. *Thin Solid Films* **2012**, *520*, 1679−1693.

(4) Street, R. A. Thin-Film Transistors. *Adv. Mater.* **2009**, *21*, 2007−2022.
(5) Mei, J.; Diao, Y.; Appeton, A. L.; Fang, L.; Bao, Z. Integrated Materials Design of Organic Semiconductors for Field-Effect Transistors. *J. Am. Chem. Soc.* **2013**, *135*, 6724−6746.
(6) Fortunato, E.; Brquinha, P.; Pimental, A.; Pereira, L.; Goncalves, A.; Martins, R. Amorphous IZO TTFTs with Saturation Mobilities Exceeding 100 cm^2/Vs. *Phys. Status Solidi RRL* **2007**, *1*, R34−R36.
(7) Liu, J.; Buchholz, D. B.; Chang, R. P.; Facchetti, A.; Marks, T. J. High-Performance Flexible Transparent Thin-Film Transistors Using a Hybrid Gate Dielectric and an Amorphous Zinc Indium Tin Oxide Channel. *Adv. Mater.* **2010**, *22*, 2333−2337.
(8) Zan, H.-W.; Yeh, C.-C.; Meng, H.-F.; Tsai, C.-C.; Chen, L.-H. Achieving High Field-Effect Mobility in Amorphous Indium−Gallium−Zinc Oxide by Capping a Strong Reduction Layer. *Adv. Mater.* **2012**, *24*, 3509−3514.
(9) Wang, L.; Yoon, M. H.; Lu, G.; Yang, Y.; Facchetti, A.; Marks, T. J. High-Performance Transparent Inorganic−Organic Hybrid Thin-Film N-Type Transistors. *Nat. Mater.* **2006**, *5*, 893−900.
(10) Sun, J.; Lu, A.; Wang, L.; Hu, Y.; Wan, Q. High-Mobility Transparent Thin-Film Transistors with an Sb-Doped SnO_2 Nanocrystal Channel Fabricated at Room Temperature. *Nanotechnology* **2009**, *20*, 335204.
(11) Kim, M. G.; Kim, H. S.; Ha, Y. G.; He, J. Q.; Kanatzidis, M. G.; Facchetti, A.; Marks, T. J. High-Performance Solution-Processed Amorphous Zinc−Indium−Tin Oxide Thin-Film Transistors. *J. Am. Chem. Soc.* **2010**, *132*, 10352−10364.
(12) Nayak, P. K.; Hedhill, M. N.; Cha, D.; Alshareef, H. N. High Performance In_2O_3 Thin Film Transistors Using Chemically Derived Aluminum Oxide Dielectric. *Appl. Phys. Lett.* **2013**, *103*, 033518.
(13) Norris, B. J.; Anderson, J.; Wager, J. F.; Keszler, D. A. Spin-Coated Zinc Oxide Transparent Transistors. *J. Phys. D: Appl. Phys.* **2003**, *36*, L105−L07.
(14) Kim, M.-G.; Kanatzidis, M. G.; Facchetti, A.; Marks, T. J. Low-Temperature Fabrication of High-Performance Metal Oxide Thin-Film Electronics via Combustion Processing. *Nat. Mater.* **2011**, *10*, 382−388.
(15) Banger, K. K.; Yamashita, Y.; Mori, K.; Perterson, R. L.; Leedham, T.; Rickard, J.; Sirringhaus, H. Low-Temperature, High-Performance Solution-Processed Metal Oxide Thin-Film Transistors Formed by a "Sol−Gel on Chip" Process. *Nat. Mater.* **2011**, *10*, 45−50.
(16) Kim, Y.-H.; Heo, J.-S.; Kim, T.-H.; Park, S.; Yoon, M.-H.; Kim, J.; Oh, M. S.; Yi, G.-R.; Noh, Y.-Y.; Park, S. K. Flexible Metal-Oxide Devices Made by Room-Temperature Photochemical Activation of Sol−Gel Films. *Nature* **2012**, *489*, 128−133.
(17) Jeong, S.; Moon, J. Low-Temperature, Solution-Processed Metal Oxide Thin Film Transistors. *J. Mater. Chem.* **2012**, *22*, 1243−1250.
(18) Thomas, S. R.; Pattanasattayavong, P.; Anthopoulos, T. D. Solution-Processable Metal Oxide Semiconductors of Thin-Film Transistor Applications. *Chem. Soc. Rev.* **2013**, *42*, 6910−6923.
(19) Park, J. H.; Kim, K.; Yoo, Y. B.; Park, S. Y.; Lim, K.-H.; Lee, K. H.; Baik, H. K.; Kim, Y. S. Water Adsorption Effects of Nitrate Ion Coordinated Al_2O_3 Dielectric for High Performance Metal-Oxide Thin-Film Transistor. *J. Mater. Chem.C* **2013**, *1*, 7166−7174.
(20) Jeong, S.; Lee, J.-Y.; Lee, S. S.; Seo, Y.-H.; Kim, S.-Y.; Park, J.-U.; Ryu, B.-H.; Yang, W.; Moon, J.; Choi, Y. Metal Salt-Derived In−Ga−Zn−O Semiconductors Incorporating Formamide as a Novel Co-solvent for Producing Solution-Processed, Elecrohydrodynamic-Jet Printed, High Performance Oxide Transistors. *J. Mater. Chem. C* **2013**, *1*, 4236−4243.
(21) Adamopoulos, G.; Thomas, S.; Wöbkenberg, P. H.; Bradley, D. D.; McLachlan, M. A.; Anthopoulos, T. D. High-Mobility Low-Voltage ZnO and Li-Doped ZnO Transistors Based on ZrO_2 High-*k* Dielectric Grown by Spray Pyrolysis in Ambient Air. *Adv. Mater.* **2011**, *23*, 1894−1898.
(22) Song, K.; Yang, W.; Jung, Y.; Jeong, S.; Moon, J. A Solution-Processed Yttrium Oxide Gate Insulator for High-Performance All-Solution-Processed Fully Transparent Thin Film Transistors. *J. Mater. Chem.* **2012**, *22*, 21265−21271.
(23) Pal, B. N.; Dhar, B. M.; See, K. C.; Katz, H. E. Solution-Deposited Sodium Beta-Alumina Gate Dielectrics for Low-Voltage and Transparent Field-Effect Transistors. *Nat. Mater.* **2009**, *8*, 898−903.
(24) Avis, C.; Jang, J. High-Performance Solution Processed Oxide TFT with Aluminum Oxide Gate Dielectric Fabricated by a Sol−Gel Method. *J. Mater. Chem.* **2011**, *21*, 10649−10652.
(25) Nomura, K.; Ohta, H.; Takagi, A.; Kamiya, T.; Hirano, M.; Hosono, H. Room-Temperature Fabrication of Transparent Flexible Thin-Film Transistors Using Amorphous Oxide Semiconductors. *Nature* **2004**, *432*, 488−492.
(26) Kamiya, T.; Hosono, H. Material Characteristics and Applications of Transparent Amorphous Oxide Semiconductors. *NPG Asia Mater.* **2010**, *2*, 15−22.
(27) Presley, R. E.; Munsee, C. L.; Park, C.-H.; Hong, D.; Wager, J. F.; Keszler, D. A. Tin Oxide Transparent Thin-Film Transistors. *J. Phys. D: Appl. Phys.* **2004**, *37*, 2810−2813.
(28) Jang, J.; Kitsomboonloha, R.; Swisher, S. L.; Park, E. S.; Kang, H.; Subramanian, V. Transparent High-Performance Thin Film Transistors from Solution-Processed SnO_2/ZrO_2 Gel-like Precursors. *Adv. Mater.* **2013**, *25*, 1042−1047.
(29) Jang, J.; Kitsomboonloha, R.; Swisher, S. L.; Park, E. S.; Kang, H.; Subramanian, V. Correction to Transparent High-Performance Thin Film Transistors from Solution-Processed SnO_2/ZrO_2 Gel-like Precursors. *Adv. Mater.* **2014**, *26*, 4412.
(30) Zhao, Y.; Dong, G.; Duan, L.; Qiao, J.; Zhang, D.; Wang, L.; Qiu, Y. Impacts of Sn Precursors on Solution-Processed Amorphous Zinc−Tin Oxide Films and Their Transistors. *RSC Adv.* **2012**, *2*, 5307−5313.
(31) Epifani, M.; Arbiol, J.; Díaz, R.; Perálvarez, M.; Sicilliano, P.; Morante, J. R. Synthesis of SnO_2 and ZnO Colloidal Nanocrystals from the Decomposition of Tin(II) 2-Ethylhexanoate and Zinc(II) 2-Ethylhexanoate. *Chem. Mater.* **2005**, *17*, 6468−6472.
(32) Anastasescu, M.; Garther, M.; Mihaiu, S.; Anastasescu, C.; Purica, M.; Manea, E.; Zaharescu, M. Optical and Structural Properties of SnO_2-Based Sol−Gel Thin Films. *Proceedings of the International Semiconductor Conference*; IEEE: Sinaia, Romania, 2006.
(33) Epifani, M.; Francioso, L.; Sicilliano, P.; Helwig, A.; Mueller, G.; Díaz, R.; Arbiol, J.; Morante, J. R. SnO_2 Thin Films from Metalorganic Precursors: Synthesis, Characterization, Microelectronic Processing and Gas-Sensing Properties. *Sens. Actuators, B* **2007**, *124*, 217−226.
(34) Jun, T.; Jung, Y.; Song, K.; Moon, J. Influences of pH and Ligand Type on the Performance of Inorganic Aqueous Precursor-Derived ZnO Thin Film Transistors. *ACS Appl. Mater. Interfaces* **2011**, *3*, 774−781.
(35) Umeda, K.; Miyasako, T.; Sugiyama, A.; Tanaka, A.; Suzuki, M.; Tokumitsu, E.; Shimoda, T. Impact of UV/O_3 Treatment on Solution-Processed Amorphous $InGaZnO_4$ Thin-Film Transistors. *J. Appl. Phys.* **2013**, *113*, 184509.
(36) Faber, H.; Butz, B.; Dieker, C.; Spiecker, E.; Halik, M. Fully Patterned Low-Voltage Transparent Metal Oxide Transistors Deposited Solely by Chemical Spray Pyrolysis. *Adv. Funct. Mater.* **2013**, *23*, 2828−2834.
(37) Dane, A.; Veldhuis, A.; de Boer, D.; Leenaers, A.; Buydens, L. Application of Genetic Algorithms for Characterization of Thin Layered Materials by Glancing Incidence X-ray Reflectometry. *Phys. B* **1998**, *253*, 254−268.
(38) Kim, D. H.; Kwon, J.-H.; Kim, M.; Hong, S.-H. Structural Characteristics of Epitaxial SnO_2 Films Deposited on a- and m-cut Sapphire by ALD. *J. Cryst. Growth* **2011**, *322*, 33−37.
(39) Elam, J. W.; Baker, D. A.; Hryn, A. J.; Martinson, A. F.; Pellin, M. J.; Hupp, J. T. Atomic Layer Deposition of Tin Oxide Films Using Tetrakis(dimethylamino) Tin. *J. Vac. Sci. Technol., A* **2008**, *26*, 244−252.
(40) Heo, J.; Kim, S. B.; Gordon, R. G. Atomic Layer Deposition of Tin Oxide with Nitric Oxide as an Oxidant Gas. *J. Mater. Chem.* **2012**, *22*, 4599−4602.

(41) Shang, J.; Liu, G.; Yang, H.; Zhu, X.; Chen, X.; Tian, H.; Hu, B.; Pan, L.; Xue, W.; Li, R.-W. Thermally Stable Transparent Resistive Random Access Memory Based on All-Oxide Heterostructures. *Adv. Funct. Mater.* **2014**, *24*, 2171−2179.
(42) Rim, Y. S.; Kim, D. L.; Jeong, W. H.; Kim, H. J. Effect of Zr Addition on ZnSnO Thin-Film Transistors Using a Solution Process. *Appl. Phys. Lett.* **2010**, *97*, 233502.
(43) Tsaroucha, M.; Aksu, Y.; Irran, E.; Driess, M. Synthesis of Stannyl-Substituted Zn_4O_4 Cubanes as Single-Source Precursors for Amorphous Tin-Doped ZnO and Zn_2SnO_4 Nanocrystals and Their Potential for Thin Film Field Effect Transistor Applications. *Chem. Mater.* **2011**, *23*, 2428−2438.
(44) Zhao, Y.; Duan, L.; Dong, G.; Zhang, D.; Qiao, J.; Wang, L.; Qiu, Y. High-Performance Transistors Based on Zinc Tin Oxides by Single Spin-Coating Process. *Langmuir* **2013**, *29*, 151−157.
(45) Ide, K.; Kikuchi, Y.; Nomura, K.; Kimura, M.; Kamiya, T.; Hosono, H. Effects of Excess Oxygen on Operation Characteristics of Amorphous In−Ga−Zn−O Thin-Film Transistors. *Appl. Phys. Lett.* **2011**, *99*, 093507.
(46) Walker, D. E.; Major, M.; Yadzi, M. B.; Klyszcz, A.; Haeming, M.; Bonrad, K.; Melzer, C.; Donner, W.; Seggern, H. V. High Mobility Indium Zinc Oxide Thin Film Field-Effect Transistors by Semiconductor Layer Engineering. *ACS Appl. Mater. Interfaces* **2012**, *4*, 6835−6841.
(47) Xia, D. X.; Xu, J. B. High Mobility and Low Operating Voltage ZnGaO and ZnGaLiO Transistors with Spin-Coated Al_2O_3 as Gate Dielectric. *J. Phys. D: Appl. Phys.* **2010**, *43*, 442001.
(48) Park, S. M.; Lee, D. H.; Lim, Y. S.; Kim, D. K.; Yi, M. Effect of Aluminum Addition to Solution-Derived Amorphous Indium Zinc Oxide Thin Film for an Oxide Thin Film Transistors. *Microlectron. Eng.* **2013**, *109*, 189−192.
(49) Cho, D.-H.; Yang, S.; Byun, C.; Shin, J.; Ryu, M. K.; Park, S. K.; Hwang, C.-S.; Chung, S. M.; Cheong, W.-S.; Yoon, S. M.; Chu, H.-Y. Transparent Al−Zn−Sn−O Thin Film Transistors Prepared at Low Temperature. *Appl. Phys. Lett.* **2008**, *93*, 142111.
(50) Lee, K.-H.; Kim, S.-M.; Jeong, H.; Pak, Y.; Song, H.; Park, J.; Lim, K.-H.; Kim, J.-H.; Kim, Y. S.; Ko, H. C.; Kwon, l. K.; Jung, G.-Y. All-Solution-Processed Transparent Thin Film Transistor and Its Application to Liquid Crystals Driving. *Adv. Mater.* **2013**, *25*, 3209−3214.
(51) Larena, A.; Millán, F.; Pérez, G.; Pinto, G. Effect of Surface Roughness on the Optical Properties of Multilayer Polymer Films. *Appl. Surf. Sci.* **2002**, *187*, 339−346.
(52) Okamura, K.; Nikolova, D.; Mechau, N.; Hahn, H. Appropriate Choice of Channel Ratio in Thin-Film Transistors for the Exact Determination of Field-Effect Mobility. *Appl. Phys. Lett.* **2009**, *94*, 183503.
(53) Xu, W.; Wang, H.; Ye, L.; Xu, J. The Role of Solution-Processed High-κ Gate Dielectrics in Electrical Performances of Oxide Thin-Film Transistors. *J. Mater. Chem. C* **2014**, *2*, 5389−5396.
(54) Cheong, W.-S.; Yong, S.-M.; Hwang, C.-S.; Chu, H. Y. High-Mobility Transparent SnO_2 and ZnO−SnO_2 Thin-Film Transistors with SiO_2/Al_2O_3 Gate Insulators. *Jpn. J. Appl. Phys.* **2009**, *48*, 04c090.
(55) Lee, D.-H.; Chang, Y.-J.; Stickle, W.; Chang, C.-H. Functional Porous Tin Oxide Thin Films Fabricated by Inkjet Printing Process. *Electrochem. Solid-State Lett.* **2007**, *10*, k51−k54.